Hybrid Modeling and Dynamics of a Controlled Reverse Flow Reactor

Erasmo Mancusi
Dipartimento d'Ingegneria, Università del Sannio, Piazza Roma, 82100, Benevento, Italy

Lucia Russo, Antonio Brasiello, and Silvestro Crescitelli
Dipartimento d'Ingegneria Chimica, Università degli Studi di Napoli "Federico II", Piazzale Tecchio 80, 80125 Napoli, Italy

Mario di Bernardo
Dipartimento di Informatica e Sistemistica, Università degli Studi di Napoli "Federico II", Via Claudio 21, 80125 Napoli, Italy

DOI 10.1002/aic.11216
Published online June 28, 2007 in Wiley InterScience (www.interscience.wiley.com).

A hybrid system approach is adopted to study the dynamic behavior of a controlled reverse flow reactor, where the occurrence of flow inversions is caused by a feedback control strategy. With this approach it is analyzed, theoretically and numerically a typical behavior of hybrid systems: Zeno phenomena. Hybrid system theory is also adopted to define a suitable Poincarè map that is a composition of two switching maps. Based on the Poincaré map an efficient methodology is developed for the continuation of limit cycles, and detection of local bifurcations as the set-point value, and inlet temperature are varied. This analysis shows that Zeno states can be coexisting with symmetric and asymmetric periodic regimes in a wide range of the parameters. The analysis of the nonlinear behavior and Zeno phenomena gives an insight on the limits of some model assumptions, and how these assumptions should be removed to avoid the unphysical response of Zeno executions. Considering a time delay due to the valves in the reactor, the unphysical Zeno state is removed, while Zeno like oscillations are shown to be still persistent. © 2007 American Institute of Chemical Engineers *AIChE J,* 53: 2084–2096, 2007

Keywords: control, mathematical modeling, hybrid system, nonlinear analysis, zeno phenomena

Introduction

Recently, the study of authothermal operation in chemical reactors, in which exothermic chemical reactions are carried out, has attracted considerable interest (see Kolios et al.[1] and references therein). In many cases it is possible to preheat the reactor feed by recovering the heat released by the reaction. However, catalytic combustion of lean mixture of VOCs (volatile organic compounds) cannot be conducted autothermally in a stationary operation without providing additional heat. In such a case periodic operations, like catalytic-reverse-flow reactor (RFR) (see for example Matros and Bunimovich[2]), are very efficient for autothermal treatment of industrial off-gas with low-concentration of VOCs.

It is well known that catalytic fixed-bed reactors can develop moving or creeping reaction fronts (see, for example, Luss[3]). In RFR, this phenomenon is exploited to conduct autothermal operation. The flow direction is reversed before

Correspondence concerning this article should be addressed to L. Russo at lucrusso@unina.it.

the front exits the reactor itself, thus, trapping the hot reaction zone inside the bed and avoiding the preheating of the feed.[2]

Two problems are related to the use of RFRs for VOCs treatment: reaction extinction and the hot spot formation due to changes in the feed conditions. To overcome the problem of the overheating different control actions have been proposed.[4–11]

Barresi and Vanni[12] proposed a feedback control to avoid reaction extinction, and keep the reaction as close as possible to optimal operating conditions (the maximum of the combustion efficiency), even in the presence of variations of the feed temperature and concentration. Temperature sensors are located at either end of the catalytic bed, and when prescribed conditions are fulfilled, the flow direction is reversed. Barresi and Vanni[12] show that this feedback control is suited even for large changes in the flow rate. The inversion of the flow direction due to the control action is modeled by Barresi and Vanni[12] as an instantaneous (discrete) transition, as its timescale is much smaller than the timescale of the reactor dynamics.

In this article, we study the dynamics and structural stability of a controlled RFR in the context of the theory of hybrid systems recently developed in the area of nonlinear dynamics and control.[13] This approach was shown to be useful to analyze many chemical processes which are modeled as hybrid systems.[14–20] We consider the control system proposed by Barresi and Vanni.[12]

The aims of this article are:

1. To model the system under investigation as a hybrid automaton and discuss the main types of solutions (or *executions*) that this model can exhibit;

2. To investigate the dynamics and the structural stability of the resulting hybrid controlled system as the set point and the inlet temperatures are changed;

3. To highlight the role of the control strategy to induce typical hybrid phenomena through numerical simulation and bifurcation analysis.

We wish to emphasize that the approach reported in this article can be used for the investigation of the dynamics of RFRs and other periodically forced chemical reactors controlled by whatever the switching control strategy. Also, it should be remarked that neglecting the hybrid nature of these systems would make impossible to correctly interpret and understand the observed dynamics.

The article is outlined as follows. We introduce the model equations of the controlled RFR, and give an interpretation of the model as a hybrid system. Then, we analyze the different types of execution exhibited by the system of interest. Special attention is given to the analysis of Zeno phenomena, a typical behavior of hybrid systems. The presence of a reflection symmetry of the system equations in both continuous and discrete variables is discussed. The system symmetry and hybrid system theory are exploited to construct appropriate Poincaré maps. Using such maps, the numerical detection of bifurcations of periodic regimes and their continuation is performed using an "*ad hoc*" numerical procedure described. Finally, the structural stability of the controlled reverse flow reactors is analyzed by performing a bifurcation analysis as the set-point temperature and the inlet temperature are changed.

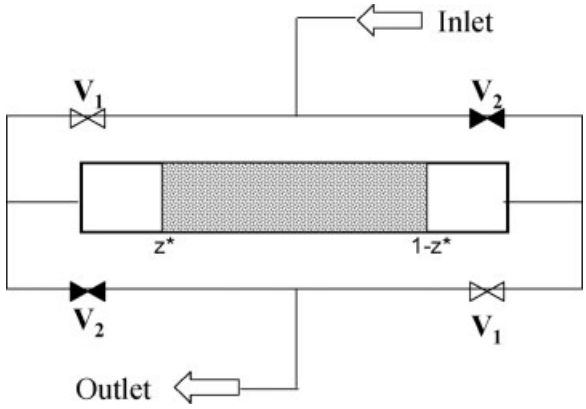

Figure 1. Reverse flow reactor.

Controlled Reverse Flow Reactors

We consider a fixed-bed reactor where a exothermic irreversible catalytic reaction takes place. As an example, the combustion of VOC over a catalytic bed is considered.

When the reactor is periodically forced, heterogeneous models must be chosen.[21] The catalytic combustor seen in Figure 1, is modeled by a one-dimensional (1-D) distributed heterogeneous model.

Such a model takes into account both heat and mass-transfer resistances between the gas and the solid phase, axial dispersion in the gas phase, axial heat conduction in the solid phase, and cooling through the reactor wall. A constant value of effectiveness factor for the reaction rate is assumed. These hypotheses are the same made by Řeháček et al.,[22] but in this work also a pseudo steady-state hypothesis for mass balance in the solid phase is assumed. The terminal parts of the bed are inert sections, and act essentially as heat exchangers.[12]

With these hypotheses, the dimensionless mass and heat balances assuming first-order exothermic reaction on the solid catalyst phase are in the form

$$\begin{cases} \dfrac{\partial y_g}{\partial t} = \dfrac{1}{Pe_m^g}\dfrac{\partial^2 y_g}{\partial z^2} + (1-2v)\dfrac{\partial y_g}{\partial z} + J_m^g(y_s - y_g) \\ \dfrac{\partial \theta_g}{\partial t} = \dfrac{1}{Pe_h^g}\dfrac{\partial^2 \theta_g}{\partial z^2} + (1-2v)\dfrac{\partial \theta_g}{\partial z} + J_h^g(\theta_s - \theta_g) - \varphi(\theta_g - \theta_w) \\ \dfrac{\partial \theta_s}{\partial t} = \dfrac{1}{Pe_h^s}\dfrac{\partial^2 \theta_s}{\partial z^2} - J_h^s(\theta_s - \theta_g) + B\eta Da(1-y_s)\exp\dfrac{\theta_s}{1+\theta_s/\gamma} \\ J_m^s(y_s - y_g) = \eta Da(1-y_s)\exp\dfrac{\theta_s}{1+\theta_s/\gamma} \end{cases} \tag{1}$$

All the symbols are explained in the Notation section. The two inert sections are described by the same equations but with no chemical reaction.

Conventional Danckwerts boundary conditions are assumed for concentration and temperature in the gas phase, while no heat conduction is considered at the reactor ends for the solid phase, that is

$$\begin{cases} \left.\dfrac{\partial y_g}{\partial z}\right|_0 - vPe_m^g y_g(0,t) = 0 \\ \left.\dfrac{\partial \theta_g}{\partial z}\right|_0 - vPe_h^g(\theta_g(0,t) - \theta_{in}) = 0 \\ \left.\dfrac{\partial \theta_s}{\partial z}\right|_0 = 0 \end{cases} \quad \begin{cases} \left.\dfrac{\partial y_g}{\partial z}\right|_1 - (1-v)Pe_m^g y_g(1,t) = 0 \\ \left.\dfrac{\partial \theta_g}{\partial z}\right|_1 - (1-v)Pe_h^g(\theta_g(1,t) - \theta_{in}) = 0. \\ \left.\dfrac{\partial \theta_s}{\partial z}\right|_1 = 0 \end{cases} \tag{2}$$

The discrete variable v takes into account the flow inversion: this variable is equal to zero when the flow direction is from left to right, and equal to one when the flow direction is from right to left. The RFR operation is shown in Figure 1.

The dimensionless variables and parameters used in Eqs. 1–2 are defined as in Řeháček et al.[22] In Table 1 these definitions are reported together with the parameter values adopted in this article. It is important to stress here that, for the parameter values used in this work, characterized by low-feed temperature and poor reactant concentration, the reactor is not able to sustain itself autothermally in the absence of flow inversions.

The state vector of the system can be represented by the vector $\mathbf{x} \equiv (y_g(z,t), \theta_g(z,t), \theta_s(z,t))$ of the spatial temperatures and gas conversion profiles, and the parameter vector by the vector $\boldsymbol{\lambda}$, which includes all the parameters of the model (see Table 1). The reactor model given by Eq 1, with the boundary conditions in Eq. 2, can be written in abstract form as the following dynamical system[23]

$$\begin{cases} \dot{\mathbf{x}} = \mathbf{F}(\mathbf{x}, v, \boldsymbol{\lambda}) & v = 0, 1 \\ \mathbf{B}(\mathbf{x}, v, \boldsymbol{\lambda}) = \mathbf{0} \end{cases} \tag{3}$$

where $\mathbf{F}$ is the right hand side of system 1, and $\mathbf{B} = \mathbf{0}$ are the boundary conditions given by the Eq. 2.

The one-point feedback control strategy proposed by Barresi and Vanni[12] is considered here for the system defined by Eq. 3. The control action reverses the flow direction when the gas temperature measured at one of the catalytic-bed edges ($\theta(z^*, t)$, when $v = 0$, and $\theta(1-z^*, t)$, when $v = 1$) decreases up to a set-point temperature (θ_{set}). It can been shown that if θ_{set} is high enough the control is able to sustain authothermally the reactor.[12] In particular, given the function

$$Q(\mathbf{x}, v, \theta_{set}) = \begin{cases} \theta_g(z^*, t) - \theta_{set} & \text{if} \quad v = 0 \\ \theta_g(1 - z^*, t) - \theta_{set} & \text{if} \quad v = 1 \end{cases} \tag{4}$$

the flow direction is reversed at time τ_i' if the following conditions are fulfilled

$$\begin{cases} Q\left(\mathbf{x}(\tau_i'), v(\tau_i'), \theta_{set}\right) = 0 \\ \left.\dfrac{\partial Q}{\partial t}\right|_{t=\tau_i'} < 0 \end{cases} \tag{5}$$

Table 1. Dimensionless Parameter and Values used in this Work

$Da = Lr_{in}/(v\varepsilon_s)$	0.56	η	1
$\gamma = E/(R\tilde{T}_{\text{in}})$	16.68	$Pe^m = Lv/D$	317.46
$Pe_{\text{g}}^{\text{m}} = \rho_g c_{pg} Lv/k_g$	644	$Pe_s^m = \rho_s c_{ps} Lv/k_s$	$1.44\ 10^5$
$J_{\text{g}}^{\text{m}} = k_m aL/(v\varepsilon)$	17.05	$J_s^m = k_m aL/(v\varepsilon_s(1-\varepsilon))$	22.9
$J_{\text{g}}^{\text{h}} = h_{fc} aL/(\rho_g c_{pg} v\varepsilon)$	28.4	$J_s^h = h_{fc} aL/(\rho_s c_{ps} v(1-\varepsilon))$	0.0227
$B = \Delta H C_{A,in}\gamma/(\rho_g c_{pg} \tilde{T}_{in})$	0.0097	y_{in}	0
$\vartheta_w = (\tilde{T}_w - \tilde{T}_{\text{in}})\gamma/\tilde{T}_{\text{in}}$	−9.6	$\phi = 4h_{fw}L/(\rho_g c_{pg} d_r v\varepsilon)$	1.2
ϑ_{in}	−9.8	ϑ_{set}	[−10;0]

Thus, the feedback control reverses the flow direction when the temperature at the control point reaches the set point temperature, but only if the temperature is decreasing. Then, if the measured temperature is below the set point value and it crosses the set point value from below, the flow direction is not reversed.

Controlled RFR as a Hybrid System

The controlled system is characterized by discrete events (the inversions of the flow direction) and continuous dynamics between two successive switches. Therefore, the RFR can be naturally analyzed as a hybrid system.[13] Specifically, the mathematical model of the controlled system is characterized by a discontinuous righthand side described by two alternating vector fields $\mathbf{F}(\mathbf{x},0,\boldsymbol{\lambda})$ and $\mathbf{F}(\mathbf{x},1,\boldsymbol{\lambda})$, with the boundary conditions $\mathbf{B}(\mathbf{x},0,\boldsymbol{\lambda}) = \mathbf{0}$ and $\mathbf{B}(\mathbf{x},1,\boldsymbol{\lambda}) = \mathbf{0}$, respectively. At each flow reversal, the righthand side changes discontinuously as a consequence of the jump of the discrete variable v, which is determined by the control law given by Eqs. 4 and 5. The flow reversal is a discrete event, and it is usually assumed to be instantaneous.[13] The dynamics between two successive flow reversals is described by a continuous dynamical model specified by the discrete variable v in Eq. 3. Thus, the controlled reactor is a nonsmooth system with discontinuous righthand side,[24] which can be classified as a hybrid system.[13] More precisely the controlled reactor consists of two different modes and a mode transition rule: One mode corresponds to a flow direction from left to right; the other corresponds to flow direction from right to left. The mode transition rule specifies when flow reversals occur. At each mode is associated a value of the discrete variable v, and at each event this discrete variable jumps from 0 to 1 or vice versa, whereas the state vector $\mathbf{x}$ evolves always continuously as a function of time. The evolution of the system will be over a time set which can been divided in time intervals as follows

$$T = \left\{ [\tau_0, \tau_0'], [\tau_1, \tau_1'], \ldots, [\tau_n, \tau_n'], \ldots \right\}, \tag{6}$$

with $\tau_i \in \mathbb{R}$ and $\tau_i' = \tau_{i+1} \leq \tau_{i+1}'$ for $i = 1, \ldots, N$. When $t \in [\tau_i, \tau_i']$, v is constant, and $\mathbf{x}$ evolves as the state of a smooth dynamical system. The set T can be a finite or infinite sequence of time intervals, and if this sequence is finite, the last time interval may have an infinite superior limit.

The set T is called hybrid time trajectory, and any collection $\chi = (v, T, \mathbf{x})$ of discrete and continuous state variables $(\mathbf{x},v)$, which evolve over the time trajectory T is called execution (see for example Lygeros et al.[25]).

Following the formalism introduced by Branicky et al.[26] a hybrid system can be modeled as a hybrid automaton; specifically, as $Ha = (V, X, Init, F, D, Guard, R)$, where:

- V is the set of the discrete variable values v, that is the set of all different modes. In our case $V = \{0,1\}$,

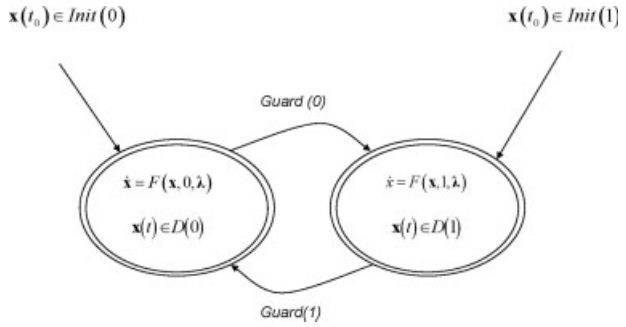

Figure 2. Hybrid automaton for the controlled RFR.

• X is the set of continuous variables, $x \equiv (y_g(z,t), \vartheta_g(z,t), \vartheta_s(z,t))$.

• *Init* is the set of initial conditions which lead to a hybrid dynamics, that is the set of initial conditions for which the control is activated at least one time during the evolution in time. In our case we have a set of initial condition for each mode, *Init*(0) and *Init*(1), both subsets of X. An example of a set of initial conditions which do not lead to a hybrid dynamics is the following: A: $\{\mathbf{x}(0) \in \boldsymbol{X} : \theta_g(z, t) < \theta_{set}\ \forall t \in \mathbb{R}, \forall z \in [0,1]\}$.

• F is the righthand side of the Eq. 3, which defines two vector fields, $\mathbf{F}(\mathbf{x}, 0, \boldsymbol{\lambda})$ and $\mathbf{F}(\mathbf{x}, 1, \boldsymbol{\lambda})$, each one for each value of the discrete variable v.

• For each v, during the continuous dynamics, the continuous state variable $\boldsymbol{x}$ cannot assume all possible values in X. $D(v)$ is, for each mode, the set of the continuous constrained values of $\boldsymbol{x}$ specified by algebraic constraints. In our case, when $v = 0$, $\mathbf{x}$ belongs to the domain[1] $D(0)$, whereas when $v = 1$, $\mathbf{x}$ belongs to the domain $D(1)$, where $D(0)$ and $D(1)$ are

$$D(0) = \{\mathbf{x} \in X : \theta_g(z^*, t) \geq \theta_{set}\}$$
$$D(1) = \{\mathbf{x} \in X : \theta_g(1 - z^*, t) \geq \theta_{set}\}.$$

• A switch condition, usually called guard condition (*Guard*), is also associated to each mode. In our case the *Guard* condition for each mode is specified by the Eq 5

$$Guard(v) = \begin{cases} Q(\mathbf{x}(\tau_i'), v(\tau_i'), \theta_{set}) = 0 \\ \left.\dfrac{\partial Q}{\partial t}\right|_{t=\tau_i'} < 0 \end{cases}$$

• R is the reset map, which assigns to the continuous state variable $\mathbf{x}$, and to the discrete variable v the new initial conditions after the occurrence of the discrete event. In our case, when the flow is reversed, the reset map acts only on the discrete variable leaving constant the continuous one

$$R : v \mapsto 1 - v$$

Thus, the action of the reset map ensures the continuity of the state variables $\mathbf{x}$.

This hybrid automaton (*Ha*) can be equivalently (more conveniently) visualized as a graph that can be easily converted into a numerical algorithm. The hybrid automaton corresponding to the controlled catalytic reactor is show in Figure 2.

This graph has as many nodes as the number of values of the discrete variable v, that is the number of modes. To each node corresponds univocally a vector field $\mathbf{F}(\mathbf{x},v,\boldsymbol{\lambda})$, a domain $D(v)$, a guard condition *Guard*(v), and a reset map $R(v)$, which reinitializes the state variables when the transition to the other mode occurs.

Therefore, the continuous state vector $\mathbf{x}$ evolves according to the differential equations system specified in the current node of the graph. When the guard condition is fulfilled, the direction of the flow is reversed, and a discrete transition takes place from one node to the other. Then, $\mathbf{x}$ is forced to satisfy the differential equations associated to the new node.

System dynamics

The controlled RFR admits different types of executions. In general, if T is an infinite sequence of intervals or if $\sum_{i=1}^{N}(\tau_i' - \tau_i) = \infty$, where N can be finite or not, the execution is called infinite, whereas if T is a finite sequence ending with a finite close interval the execution is called finite.[25,27] The execution time $T(\chi)$ is defined as $T(\chi) = \sum_{i=1}^{N}(\tau_i' - \tau_i)$. A typical infinite execution with an infinite execution time, and $N = \infty$ is a periodic regime. The control acts periodically reversing the flow direction, and is able to sustain autothermally the reaction.

In Figure 3 an infinite execution with an infinite execution time, but with a finite number of events ($N = 2$) is reported. This execution leads to a nonignited regime. The hybrid time trajectory is now constituted by a finite number of intervals,

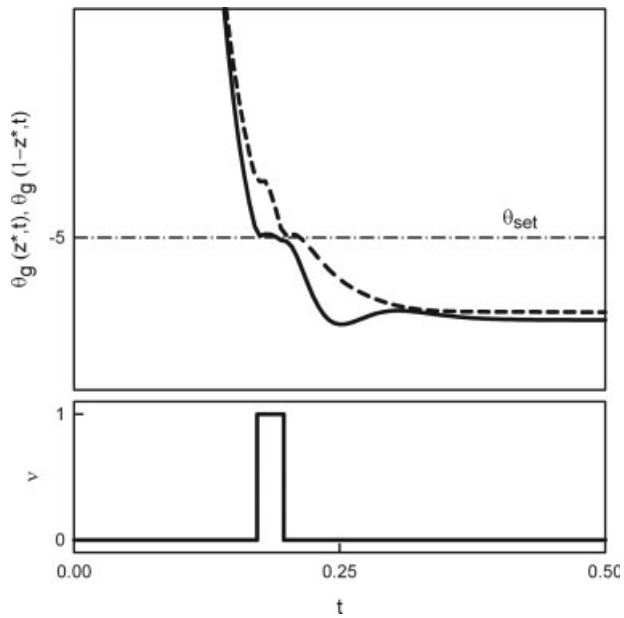

Figure 3. The uppermost plot shows the temperature evolution ($\theta(1-z^*,t)$ solid line, $\theta(z^*,t)$ dashed line), and the lower most plot reports the evolution of the discrete variables v vs. t.

These results are obtained for $\theta_{set} = -5$. For the sake of clarity only the transient behavior is shown.

[1]The domain is sometimes called the invariant set, especially in the hybrid systems literature in computer science.[25] The invariant set is not invariant in the sense of dynamical system theory.

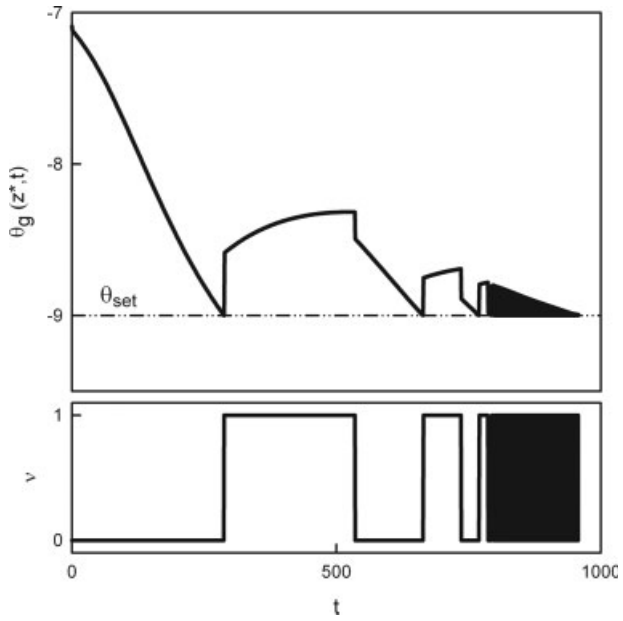

Figure 4. The uppermost plot shows the temperature evolution $\theta(z^*,t)$, and the lower most plot reports the evolution of the discrete variables v vs. time t.

These results are obtained for $\theta_{set} = -9$.

the last of which has an infinite superior limit. Indeed, as shown in Figure 3, after the second inversion both measured temperatures are below the set point value. Then, the control law acts just twice, and the system evolves indefinitely following the dynamics of one mode. In this case the control is not able to trap the heat of the reaction, and the system reaches a nonignited steady-state regime condition in an infinite time.

Zeno executions

The Zeno phenomenon is fundamentally a hybrid phenomenon.[28–30] While for continuous systems, time series can be extended over an arbitrary long-time horizon, a hybrid system can exhibit a time series where an infinite number of discrete events takes place in finite time. The associated time series is termed as a Zeno execution and hybrid systems that accept such executions are referred as Zeno hybrid automata (see for example 25, 29–31).

In hybrid systems theory, a necessary condition for the existence of Zeno executions is that the graph is a cycle (proposition 5 in Ref. 29). In our case, such condition is satisfied (Figure 2), and, thus, the controlled reverse flow reactor may have Zeno executions. It is worth to note that, in our case, the reset map (R) acts on the state variable $\mathbf{x}$ as an identity map, and such condition ensures that a Zeno execution exists, and it is unique (proposition 6 and theorem 2 in Ref. 29).

A numerical example of a Zeno execution is reported in Figure 4. In this case the system exhibits an execution with an infinite number of discrete events ($N = \infty$), but a finite execution time T_∞ (Zeno time[29,30]). As shown in Figure 4, in a Zeno execution the flow direction is reversed more and more frequently with an infinite number of switches accumulating in a finite time equal to T_∞. In our case, the Zeno state (the state attained at T_∞) corresponds to conditions in which $\theta_g(z^*, t) = \theta_g(1 - z^*, t) = \theta_{set}$ and $T_\infty \approx 957$ (which is numerically evaluated, and in general depends from the initial conditions[29]). In such condition the control system switches at higher and higher frequency, trying to segregate the necessary heat to sustain autothermally the process. Because of the low-feed temperature, the heat produced by the reaction is not enough to sustain autothermally the process for the chosen initial conditions. On the other hand the control policy implies that the measured temperature cannot be lower than the set point value, then a condition in which the set-point temperature is equal to the measured temperature is reached with an infinite frequency of switches. Thus, physically, the system should reach a nonignited regime, but the control law and the mathematical model do not allow the system to evolve over a time larger then the Zeno time.

Moreover, being the continuous part of R the identity, the reset map is not expanding, therefore, the Zeno state belongs to the intersection of the boundaries of the domains $D(0)$ and $D(1)$ (proposition 7 in Ref. 29). Given the two boundaries

$$\partial D(0) = \{\mathbf{x} \in X : \theta_g(z^*, t) = \theta_{set}\}$$
$$\partial D(1) = \{\mathbf{x} \in X : \theta_g(1 - z^*, t) = \theta_{set}\}$$

it follows that the Zeno state $\mathbf{x} = Z_\infty \in \partial D(0) \cap \partial D(1)$, and, thus $\theta_g(z^*, t) = \theta_g(1 - z^*, t) = \theta_{set}$. This theoretical consideration is confirmed by the numerical results discussed before.

"Regularization" of Zeno executions

The Zeno phenomenon is unphysical and it is due to the model simplifications. However, it is important to be able to determine if a hybrid system exhibits Zeno trajectories, because their understanding can help in to identify the hypotheses to be removed.

For the controlled RFR the Zeno phenomenon is due to the assumption of an instantaneous flow inversion. In order to remove the Zeno phenomenon, we consider a time lag $\varepsilon > 0$, between the time at which the measured temperature reaches the set-point value, and the time at which the inversion of the flow direction occurs. This time lag takes into account characteristic times of the control measures and the valves system.

The strategy used in this article in order to remove the Zeno phenomenon is called by Johansson et al.[27] "temporal regularization". In Figure 5 a numerical simulation of the regularized system is reported. In the cases represented in Figure 5 we use two values of the time delay $\varepsilon = 1$ (Figure 5a), and $\varepsilon = 10$ (Figure 5b). As it is apparent, after a short transient that shows many high-frequency switches, the reactor temperature decreases until the extinction of the reaction. Then, although the Zenoness is removed, the high-frequency (Zeno-like) oscillations are not completely removed. As reported in Figure 5 the longer the time delay (ε) is chosen, less high-frequency oscillations are observed in the regularized system.

It should be noted that the assumption of an instantaneous flow inversion cannot be used only when the switching fre-

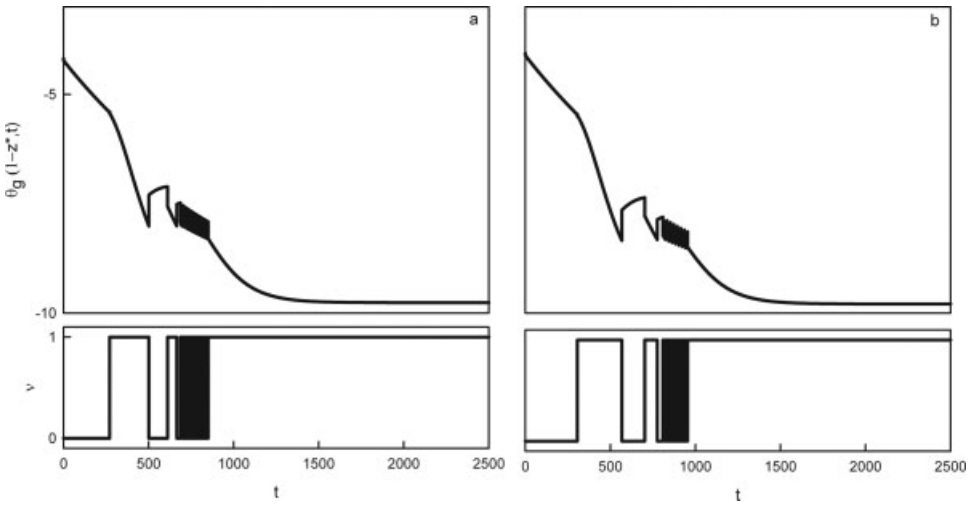

Figure 5. The uppermost plot shows the temperature evolution θ (1 − z^*,t), and the lower most plot reports the evolution of the discrete variables v vs. time t.

These results are obtained for $\theta_{set} = -8$, and (a) $\varepsilon = 1$, and (b) $\varepsilon = 10$.

quency is too high respect to the characteristic times of the measure control and the valves system, as in the case of Zeno phenomena. However, even if this assumption is removed the controlled RFR may exhibit high-frequency oscillations (Zeno-like) which could damage the control system.

System symmetry

As we will see, the controlled RFR under investigation admits executions corresponding to asymmetric and symmetric periodic regimes as in the case of the uncontrolled RFR. In the latter case, the symmetry of these periodic regimes is a spatio-temporal one[32,33] and it can be expressed as follows

$$\mathbf{x}(z,t) = \mathbf{x}(1-z, t+T/2), \tag{7}$$

where T is the forcing period and $T/2$ is the time between two successive switches. Russo et al.[33] observed that the regime symmetry is due to the spatiotemporal symmetry of the model equations induced by the periodic forcing.

The controlled RFR here considered is an autonomous (hybrid) system, and, therefore, cannot have spatiotemporal symmetry. The symmetry of controlled RFR is here induced by the feedback control law, which reverses the flow direction according to the value of the system states. Therefore, the invariance properties of the symmetric regimes have to include also the control law. Defining the following transformations

$$G : \mathbf{x}(z,t) \in X \rightarrow \mathbf{x}(1-z,t) \in X \tag{8}$$

$$g : v \in V \rightarrow 1 - v \in V, \tag{9}$$

it appears that the controlled system of Eqs. 3–4 is invariant with respect to a symmetry group $\Gamma = \{G,I\}\times\{g,1\}$, which is homeomorph to $\mathbb{Z}_2 \times \mathbb{Z}_2$.[34]

In fact, the application of the couple (G, g) to the controlled system of Eqs. 3–4 leaves the system invariant

$$G \otimes gF(\mathbf{x}, v) = F(G(\mathbf{x}), g(v)) \tag{10}$$

$$G \otimes gB(\mathbf{x}, v) = B(G(\mathbf{x}), g(v)) \tag{11}$$

$$Q(\mathbf{x}, v) = Q(G(\mathbf{x}), g(v)). \tag{12}$$

In Eqs. 10–11, $G \otimes g$ is the homeomorphism acting on ($\mathbf{x}$,v) $\in X \times V$ defined by Eqs. 8 and 9.

Thus, the symmetry transformations, in this case, do not involve the time, but only the continuous and discrete variables: it is a spatial symmetry.

Existence and stability of periodic regimes

We now investigate the existence and stability of periodic solutions exhibited by the reactor under investigation. As shown following, the analysis is simplified by the aforementioned symmetry of the system. Moreover, due to the discontinuity of the vector field, the closed-loop system dynamics cannot be studied with standard tools for smooth systems. To overcome this problem, we need to construct a suitable Poincaré map which stems from the hybrid system theory.

Symmetric Periodic Regimes. It is well known[35] that time-continuous symmetric systems can have both symmetric and asymmetric regimes. In particular periodic regimes can be point-wise invariant or set-wise invariant with respect to a symmetry group Γ. In the first case the solution $\mathbf{x}(t)$ verifies that $\mathbf{x}(t) = \gamma\mathbf{x}(t) \forall t, \forall \gamma \in \Gamma$, whereas in the second case, if C is the orbit in the phase space, then $C = \gamma C$.

In our case, the symmetric periodic regimes respect the Eq. 7 as the uncontrolled case, where $T/2$, the switch time, is now chosen by the control law.

Then these regimes cannot be point-wise invariant: They are set-wise invariant, that is

$$G(C) = C. \tag{13}$$

This property is shown in Figure 6a, where a projection of a symmetric periodic orbit is reported.

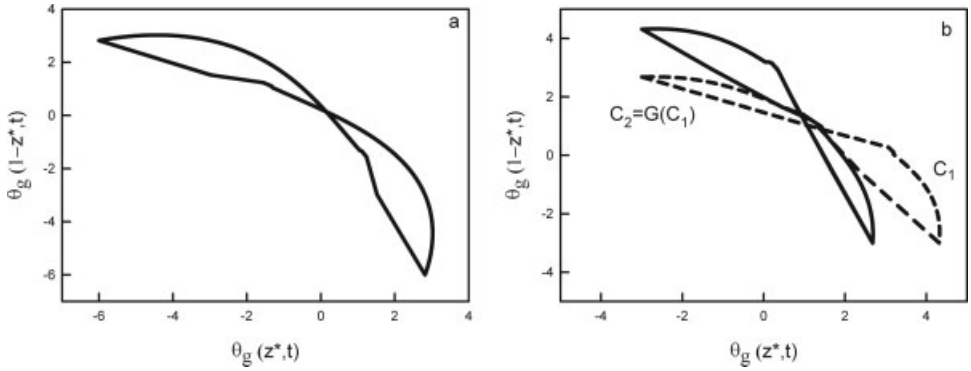

Figure 6. Projection of the periodic orbit in the plane ($\theta_g(z^*,t)$, $\theta_g(1-z^*,t)$): (a) symmetric periodic orbit obtained for $\theta_{set}=-6.0$, and (b) two G-Conjugate aymmetric periodic orbits obtained for $\theta_{set}=-3$.

The properties stated by Eqs. 10–12 imply that, if $\mathbf{x}(t)$ is a system execution, $G\mathbf{x}(t)$ is a system execution too. Therefore, if an asymmetric periodic regime exists, then symmetry implies the coexistence of two G-conjugated periodic asymmetric regimes that satisfy the following property

$$\begin{aligned} G(C_1) &= C_2 \\ G(C_2) &= C_1 \end{aligned} \tag{14}$$

In Figure 6b two G-conjugate asymmetric regime orbits are plotted, and the properties Eq. 14 can be easily verified.

Construction of Poincaré maps

The transition from symmetric to asymmetric regimes is marked by symmetry-breaking bifurcations and complex bifurcations may appear if a system parameter is changed. In order to perform a detailed bifurcation analysis, an appropriate methodology for hybrid systems is needed.

Indeed, due to the discontinuity of the vector field, the closed-loop system dynamics cannot be studied with standard tools for smooth systems.

For autonomous systems the Poincaré maps have a local meaning, and their construction is not trivial because of the difficulties in the identification of Poincaré sections. For hybrid systems, maps have been defined which are useful to understand the underlying system dynamics,[36,37] and are useful to construct Poincaré maps. In our case, the so-called switching map can be easily constructed by sampling the state of the system at every switch. In Figure 7 an orbit projection of a (symmetric) periodic regime is reported. When the control action reverses the flow direction, the continuous state vector belongs to a hyperplane ($\mathbf{x}_0 \in S_0$). Then the orbit evolves following the continuous dynamics for $v = 0$ until it impacts a second hyperplane ($\mathbf{x}_1 \in S_1$), when the guard condition is again fulfilled. Then the orbit evolves following the dynamics for $v = 1$ until it closes on itself on the hyperplane S_0.

It is apparent that two different switching maps can be considered.[37] These maps can be defined considering the intersections between the system trajectories, and the two (switching) hyperplanes defined as

$$\begin{aligned} S_0 &= \{\mathbf{x} \in X, Q(\mathbf{x},0) = 0\} \\ S_1 &= \{\mathbf{x} \in X, Q(\mathbf{x},1) = 0\} \end{aligned}. \tag{15}$$

For the switching maps, the intersections to be considered are only those corresponding to switch caused by the control feedback law (Eq. 5). Therefore, if $\boldsymbol{x}_0$ is the intersection of a T-periodic orbit with the switching hyperplane S_0, the two switching maps can be defined as

$$\Pi^+ : \mathbf{x} \in D(0) \subseteq S_0 \rightarrow \Phi_{t(\mathbf{x},0)}(\mathbf{x}) \in D(1) \subseteq S_1, \tag{16}$$

$$\Pi^- : \mathbf{x} \in D(1) \subseteq S_1 \rightarrow \Phi_{t(\mathbf{x},1)}(\mathbf{x}) \in D(0) \subseteq S_0. \tag{17}$$

Here $\Phi_{t(\mathbf{x},v)}$, is the evolution operator of the controlled system Eqs. 3–4. Choosing S_0 as Poincaré section, the Poincaré map can be expressed as the composition of Π^+ and Π^-

$$P_0 = \Pi^- \circ \Pi^+. \tag{18}$$

Similarly, choosing S_1 as Poincaré section, another Poincaré map can be defined as

$$P_1 = \Pi^+ \circ \Pi^-. \tag{19}$$

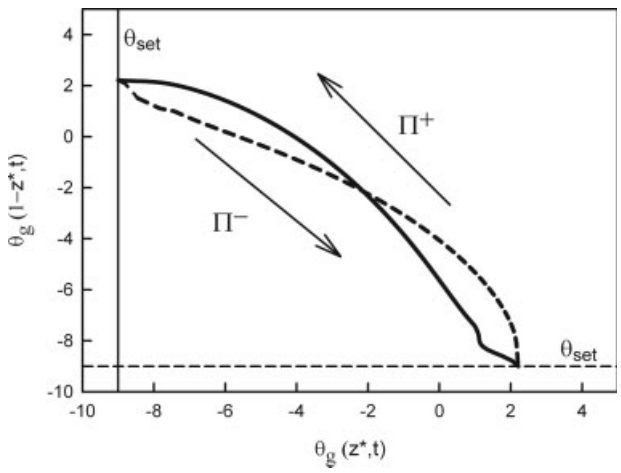

Figure 7. Projection of the periodic orbit in the plane ($\theta(1-z^*,t)$, $\theta(z^*,t)$) obtained for $\theta_{set}=-9.0$.

The solid curve represents the orbit projection for $v = 0$, while the dashed curve represents the orbit projection for $v = 1$. The solid line is the projection of S_0 hyperplane and the dashed line is the projection of S_1 hyperplane.

Considering that

$$S_0 = GS_1 \qquad S_1 = GS_0 \tag{20}$$

both Poincaré maps defined in Eqs. 18–19, can be written as the second iterate of another map H_0 or H_1, respectively. In fact

$$P_0 = G \circ \Pi^+ \circ G \circ \Pi^+ = (G \circ \Pi^+)^2 = (H_0)^2 \qquad P_1 = G \circ \Pi^- \circ G \circ \Pi^- = (G \circ \Pi^-)^2 = (H_1)^2 . \tag{21}$$

From now on, we will refer to the Poincaré section S_0, and for the sake of clarity we will indicate with P the relative Poincaré map, and with H the related map defined in Eq. 21.

Fixed points of the Poincarè map and their stability

For a T-periodic orbit, it follows that

$$P(\mathbf{x}_0) = \Pi^- \circ \Pi^+(\mathbf{x}_0) = \mathbf{x}_0 \quad \text{and} \quad t(\mathbf{x},0) + t(\mathbf{x},1) = T \tag{22}$$

The symmetry properties of the periodic regime can be easily deduced by the relation between the fixed points of the Poincaré map and the fixed points of the H map. In particular, a symmetric periodic orbit corresponds to a fixed point of both maps.

$$P(\mathbf{x}_0) = H(\mathbf{x}_0) = \mathbf{x}_0 \quad \text{and} \quad t(\mathbf{x},0) = t(\mathbf{x},1) = T/2 \tag{23}$$

Whereas, in the case of asymmetric T-periodic regime, the fixed points of the Poincaré map are not fixed points of the H map, and the switch times are not constant anymore

$$P(\mathbf{x}_0) = \mathbf{x}_0,\ H(\mathbf{x}_0) \neq \mathbf{x}_0, \quad \text{and} \quad t(\mathbf{x},0) + t(\mathbf{x},1) = T \text{ but } t(\mathbf{x},0) \neq t(\mathbf{x},1) \tag{24}$$

The proofs that a symmetric periodic regime is characterized by Eq. 23, and that an asymmetric regime is characterized by Eq. 24, are similar to those reported by Kutznetzov,[35] except from the definition of the map H now given by Eq. 21.

Once a suitable Poincaré map has been defined, the stability of a periodic orbit of the system is assessed by studying the stability of the corresponding fixed point of the P map. The stability of the periodic regime (both symmetric and asymmetric) is governed by the eigenvalues of the Jacobian matrix of the Poincaré map (Floquet multipliers). A periodic regime is stable if all eigenvalues are inside the unit circle in the complex plane. Whenever one or more eigenvalues cross the unit circle, the periodic regime becomes unstable. Depending on the crossing position, different types of local smooth bifurcations are possible.[35] It should be noted that although the righthand side of the system 3–4 is discontinuous, in correspondence of periodic regimes, the local Poincaré map defined in Eq. 21 is smooth, and then the bifurcation analysis of the limit cycles can be conducted applying the standard tools for discrete time systems.

Symmetric regimes cannot possess all bifurcations that an asymmetric periodic solution may have, as Eq. 21 poses some constraints. Particularly, symmetric regimes cannot exhibit generic flip bifurcations.[38] Moreover, nongeneric bifurcations, such as pitchfork bifurcations become generic.[35,39,40] In fact, as it will be shown in the following, pitchfork bifurcations represent the main mechanism of loss of symmetry for the controlled RFR here considered.

The bifurcations of the fixed points of the H map are related to the bifurcations of the fixed points of the P map. Eq. 23 dictates correspondences between the two maps and their bifurcations. Since $P = H(H(\mathbf{x}_0))$, the Jacobian matrix of the P map is related to that of the H map by the following obvious relationship

$$D_{\mathbf{x}}P = D_{\mathbf{x}}\,H\Big|_{H(\mathbf{x}_0)}\, D_{\mathbf{x}}\,H\Big|_{\mathbf{x}_0} \tag{25}$$

and, if $\mathbf{x} = \mathbf{x}_0$ is a fixed point of the H map, it follows

$$\boldsymbol{D}_{\mathbf{x}}\,P\Big|_{\mathbf{x}_0} = \left(D_{\mathbf{x}}\,H\Big|_{\mathbf{x}_0}\right)^2 \tag{26}$$

Thus, the Floquet multipliers of $\mathbf{x}_0$ correspond to the square eigenvalues of the Jacobian matrix of the H map in $\mathbf{x}_0$. As a consequence, if the Jacobian matrix of the H map has an eigenvalue equal to -1 (flip bifurcation), then the Jacobian matrix of the P map has a corresponding Floquet multiplier equal to $+1$ (pitchfork bifurcation).

Numerical continuation techniques

The numerical analysis of Eqs. 1–2 has been performed reducing the PDEs system to a set of 60 ODEs by orthogonal collocation technique on finite elements.[41] In fact, we have verified that, if the domain of the reactor is divided in three blocks and 20 collocation points are used over the three blocks, the discretization is enough to obtain accurate results.

The computation of the solution branches, their stability and the bifurcations detection are done by embedding into the continuation software an external time-stepper integrator that numerically computes the Poincaré map. As mentioned before, the dynamics of the controlled RFR can be studied through the discrete-time dynamics of the Poincaré map P, or via the H map earlier defined (Eq. 21). It is important to observe that both maps are smooth and invertible in that they are composed by diffeomorphisms.[35] This property overcomes the problems related to the discontinuity of the vector field in the underlying continuous time system. Continuation algorithms can then be applied to the discrete-time system.

As continuation algorithm, in this context we choose the one implemented in AUTO 97.[42] AUTO can trace the fixed points locus of a discrete map, given an initial point of this locus. AUTO can also compute branches of stable and unstable fixed points for a discrete system, and compute the Floquet multipliers that determine the stability along these branches and the local bifurcations. It is worth noting that

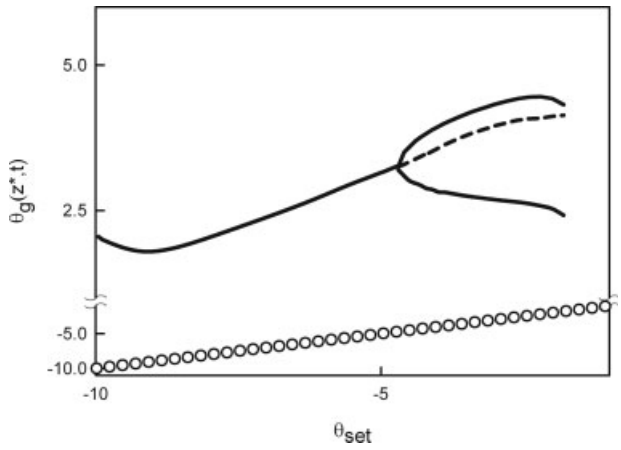

Figure 8. Solutions diagrams of periodic regimes with the set-point temperature as the bifurcation parameter.

As the representation of the state is chosen, the variable $\theta_g(z^*, t)$. In the solutions diagram the bifurcation parameter is the set-point temperature and stable periodic regimes are shown as solid lines, and unstable regimes are shown as dashed lines. Zeno states are reported with empty circles. Of course the Zeno states branch is obtained through numerical simulation.

AUTO also contains an algorithm for branch switching. This is specially useful in our case, in that it allows automatic continuation of asymmetric solution branches stemming from pitchfork bifurcations.

Standard use of AUTO requires that the user supplies an analytic expression of the discrete-time system. Namely, the righthand-side of the map Eq. 21 must be implemented in the user-defined subroutine FUNC. In our case this is not straightforward, since an analytic expression for the map is unavailable. Therefore, we must resort to numerical evaluation of our maps. The proposed technique consists of an interaction between AUTO (or any equivalent continuation software) and an ODE solver, which efficiently evaluates numerically the map. It is worth noting that the time integration has to be performed connecting a standard time-step integrator (LSODE[43]) with a specific event-driven subroutine (DA2CJF from the NAG toolbox) for an accurate detection of the time value and the state of the system at the time inversion, as dictated by the control rule. To perform an accurate time integration it is necessary to detect correctly the time τ_j' at which the discrete event occurs, and the value of the state of the system in τ_j'. The software LSODE is not accurate enough to detect the instant τ_j'. The DA2CJF subroutine integrates a system of first-order ordinary-differential equations over a range with suitable initial conditions, using a variable-order, variable-step Adams method until a user-specified function is zero, and returns the solution at points specified by the user, if desired.

The map is supplied to AUTO within the subroutine FUNC, where AUTO holds all function definitions. The vector state of the system is sent to the integrator, which sends it back after a time equal to τ, for the one-iterate.

The symmetric regimes are obtained by continuing fixed points of the H map in order to reduce the time needed for the computation, while the T-periodic asymmetric regimes are obtained by continuing fixed points of the P map.

Bifurcation Analysis

Here, we study the influence of the set-point temperature and the inlet temperature on the dynamic behavior of the controlled RFR. Varying both the parameters the controlled RFR shows a very complex behavior: symmetric and non-symmetric periodic regimes have been detected, and these regimes coexist with Zeno executions.

Evidence of such coexistence is shown in Figure 8, where the solution diagram is depicted with the set-point temperature θ_{set} as bifurcation parameter. All solution branches correspond to T-periodic regimes. The periodic regimes are represented by the value of the gas temperature at the reactor exit.

For low-value of the set-point temperature the controlled RFR exhibits stable periodic symmetric regimes. Spatial profiles of a symmetric periodic regime are reported in Figure 9a, where it is evident that the profile at instant $t + T/2$ is a mirror reflection of the profile at instant t, consistantly with Eq. 7.

In symmetric regimes, two symmetric positions (z and $1 - z$, respectively) within the reactor, experience the same time series, but with a time shift equal to $T/2$. As the set

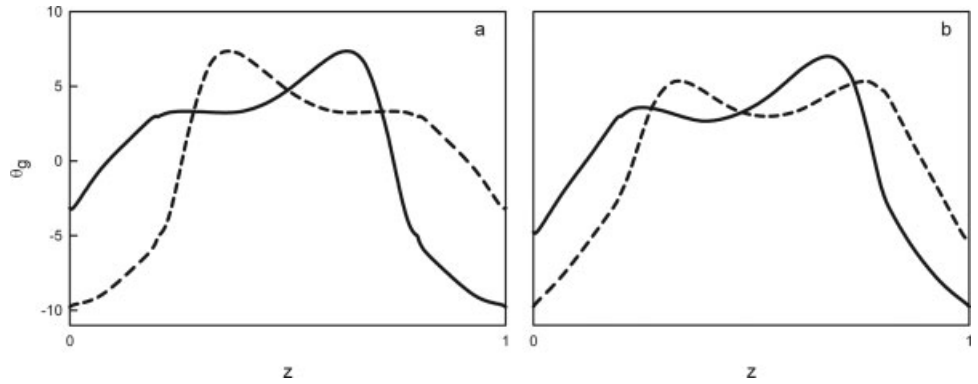

Figure 9. (a) Spatial gas-temperature profiles at time t and $t+ T/2$ of a symmetric periodic regime, $\theta_{set} = -6$, and (b) spatial gas-temperature porfiles at time t and $t+ T/2$ of an asymmetric periodic regime, $\theta_{set} = -2$.

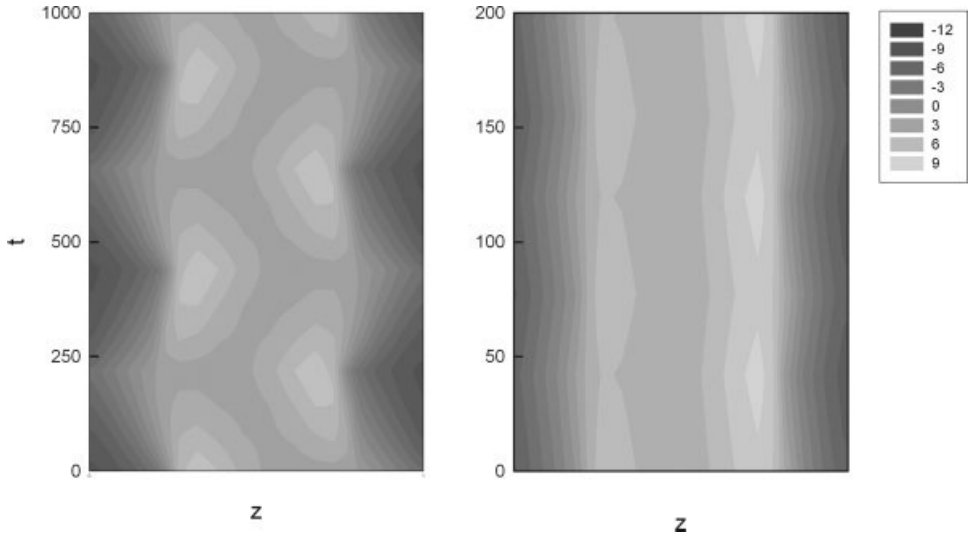

Figure 10. Spatiotemporal patterns of the temperature in the solid phase.

(a) $\theta_{set} = -6$, and (b) $\theta_{set} = -2$. The correspondence between the level of temperature, and the color scale is reported in the figure legend.

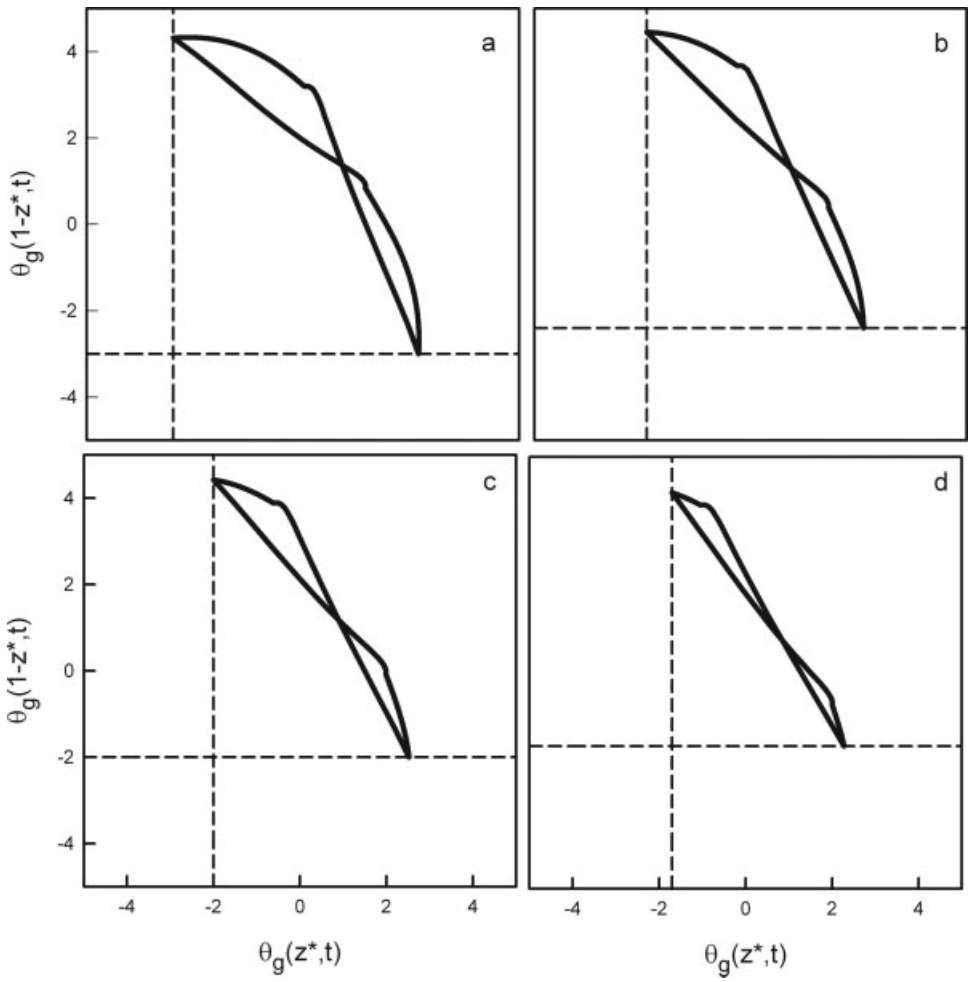

Figure 11. The projection of the periodic orbit in the plane ($\theta(1 - z^*,t)$, $\theta(z^*,t)$) obtained for (a) $\theta_{set} = -3$, (b) $\theta_{set} = -2.4$, (c) $\theta_{set} = -2$, and (d) $\theta_{set} = -1.7$.

The solid curve represents the orbit projection, while the dashed curve represents the projections of the hyperplane S_0 and S_1. The period regimes are respectively: (a) 260, (b) 175, (c) 77, and (d) 37.

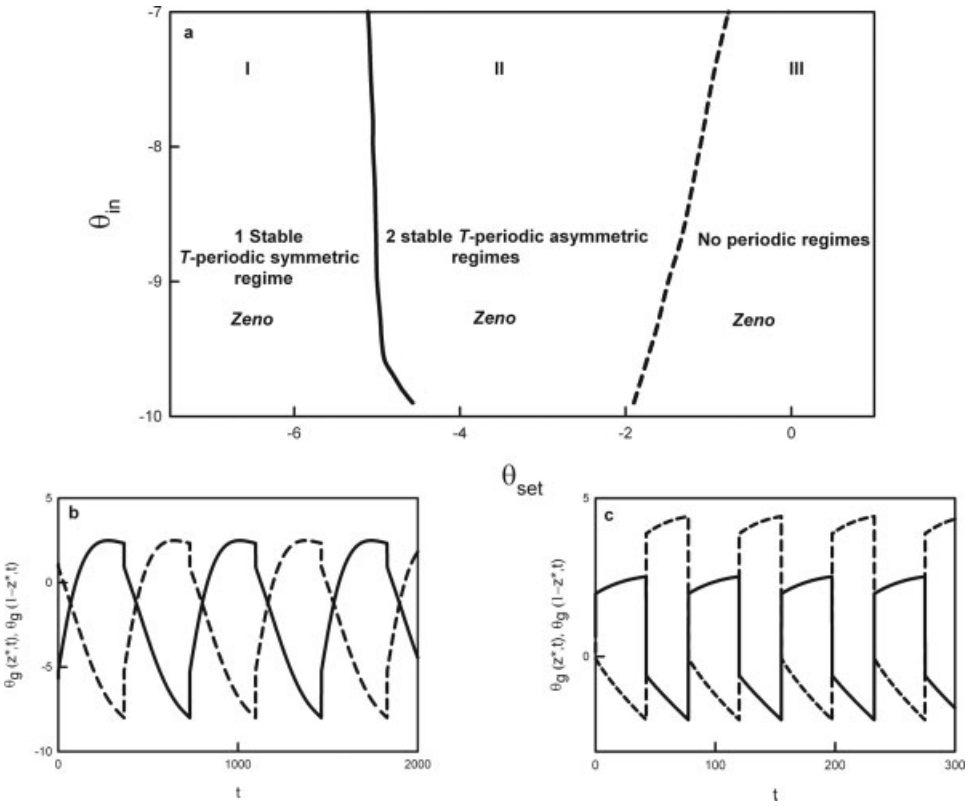

Figure 12. (a) Bifurcation diagram: the solid curve represents the locus of pitchfork bifurcation, and the dashed curve represents the locus of global bifurcation, (b) shows the temperature evolution ($\theta(1 - z^*,t)$ solid line, $\theta(z^*, t)$ dashed line) for symmetric T-periodic regime at $\theta_{set} = -8$, and $\theta_{in} = -9.8$, and (c) shows the temperature evolution ($\theta(1 - z^*,t) - \theta(z^*,t)$ dashed line) for asymmetric *T*-periodic regime at $\theta_{set} = -2$ and $\theta_{in} = -9.8$.

point temperature is increased until $\theta_{set} = -4.7$ ($\approx$250°C), the system exhibits a supercritical pitchfork bifurcation. In correspondence of the pitchfork bifurcation the symmetric *T*-periodic regime becomes unstable and two *G*-conjugate stable asymmetric *T*-periodic regimes emerge. In Figure 9b spatial profiles of an asymmetric regime at two successive switch instant values are reported. It is evident that the profile at instant $t + T/2$ is not a mirror reflection of the profile at instant t. It can be observed that asymmetric *T*-periodic regimes are characterized by different time series at two symmetric positions within the reactor (z and $1 - z$). Moreover, the time intervals between two successive switches in the asymmetric periodic regimes are not equal (see Eq. 24).

The physical effect of the spatiotemporal symmetry breaking is evident from the analysis of the spatiotemporal patterns. Figure 10 shows the spatiotemporal pattern of the solid temperature. The temperature level is color coded, the nondimensional axial coordinate is reported in abscissa, and the time (t) in ordinate. In Fig 10a a spatiotemporal pattern of a *T*-periodic symmetric regime is shown, and its spatiotemporal symmetry properties dictated by Eq. 7 clearly appear. In a symmetric regime the hot zone is equally distributed with respect to the reactor center. Indeed, the left and right part of the reactor experience the same spatial profiles evolution. In the case of *T*-periodic asymmetric regime Figure 10b, the spatiotemporal pattern is such that the right portion of the catalytic bed is, in average, hotter. On the contrary, when the reactor operates in the coexisting *G*-conjugate periodic regime, the left part is in average hotter than the right part.

For the θ_{set} ranging from the ambient temperature to -1.67 ($\approx$384°C) one or more *T*-periodic regimes coexist with Zeno state. Therefore, different initial conditions belonging to the domain $D(0)$ and $D(1)$ may lead to a Zeno execution or to a *T*-periodic regime. For continuous dynamical systems different methods are available in order to define the basin of attraction of stable regimes. These regions can be identified, for example, by means of stable manifolds of a saddle limit set or with the use of Lyapunov functions. However, for hybrid system and in particular for the Zeno state there is no general theory other than the brute force approach to identify the basin of attraction.

In Figure 11 we report the projection of an asymmetric *T*-periodic regime as the set point value is increased. We observe that the period and the amplitude of the oscillations regimes decrease and, in the phase space, the average distance between the Zeno state and the orbit decreases too.

For set-point temperature greater than -1.67, only the Zeno state is found. We conjecture that disappearance of the two asymmetric periodic regimes is caused by a global bifurcation due to the interaction of the asymmetric periodic orbit with the attraction basin of the Zeno state.

We finally note that the time regularization previously discussed does not affect the bifurcation scenario of the system discussed in Figure 8. The only found difference is that the

Zeno state is replaced by a nonignited regime, which could be reached with transient Zeno-like oscillations. Then a suitable startup policy should be adopted to avoid the transient Zeno-like oscillations which coexists with the desired periodic regime.

The dependence on θ_{in} of the pitchfork bifurcation (Figure 8), which marks the appearance of stable T-periodic asymmetric regimes, can be determined with two parameter continuation setting θ_{in} and θ_{set}, as bifurcation parameters. Figure 12a shows in the plane $(\theta_{in},\theta_{set})$ the loci of the pitchfork bifurcation (solid line), and the loci of the global bifurcation point (dashed line), which leads to the disappearance of the stable T-periodic regimes. These two loci delimit the regions in the plane $(\theta_{in},\theta_{set})$, where different kind of regimes can be found.

The Zeno state exists in all the investigated parameters range. Particularly, in region **III** in Figure 12a the Zeno state is the only possible regime, whereas in regions **I** and **II** it coexists with symmetric and asymmetric T-periodic regimes, respectively. Typical time series of T-periodic regimes are reported in Fig 12b for the symmetric regimes, and in Figure 12c for the asymmetric regimes. It is worth to note that the region **I** is the more suitable operative region for stable periodic operations. Although in such region the Zeno state exists, startup conditions with the fixed bed hot enough will lead to stable and symmetric periodic regimes.

Conclusions

We used an hybrid system approach for a controlled reverse flow reactor to study the dynamical behavior of the closed-loop system as the set-point, and the inlet temperature are varied. The control consists of a feedback control law, which reverses the flow direction when the temperature measured by sensors located at either end of the catalytic bed falls below a fixed value.

The hybrid automaton of the system is defined and the system symmetry properties are discussed. It is shows that the system shares a rich variety of executions corresponding to symmetric and asymmetric periodic regimes, extinction regimes with a finite number of switches and Zeno executions with infinite number of switches occurring in finite time.

We found that, Zeno or Zeno-like executions are coexisting with stable periodic symmetric and asymmetric regimes in all the investigated parameter range. We characterize these regimes and their bifurcations with an "*ad hoc*" continuation technique, based on the Poincaré map constructed as composition of two switching maps of the system. The developed technique exploits the symmetry and the hybrid properties of the system. Most interestingly, this technique can be applied by means of a combination of popular and robust pieces of software, that is an automatic continuation package (AUTO97), an ODE package (LSODE), and a event-driven subroutine (DA2CJF).

We wish to emphasize that the hybrid system approach adopted here is essential to understand the dynamics of switched systems, and the reliability of their mathematical model in different operating conditions. Moreover, the strategy used in this article to analyze the simple RFR and the properties of Zeno and periodic executions can also be used to analyze more complicated systems or control strategies, where on a macroscopic time-scale, the controller switches between different configurations. In this sense the theorems and the theoretical results used in this article are completely general.

Acknowledgments

This work was partially funded by MIUR, and CNR (Gruppo Nazionale per la Difesa dai Rischi Chimico-Industriale ed Ecologici).

Notation

a = catalyst external surface area
c_p = heat capacity
C_A = concentration of the specie A
d_r = reactor diameter
D = mass axial-dispersion coefficient
E = activation energy
$f(t)$ = forcing function
G = linear operator defined in Eq. 8
g = linear operator defined in Eq. 9
h_{fc} = heat-exchange coefficient between gas phase and catalyst
h_{fw} = heat-exchange coefficient between gas phase and reactor wall
k_0 = Arrhenius constant
k_g = gas-phase axial heat conductivity
k_m = mass-transfer coefficient
k_s = solid-phase axial heat conductivity
I = identity operator
L = reactor length
P = Poincaré map defined in Eq. 18
Q = control law defined in Eq. 5
R = gas constant
r = reaction rate
S = hyperplane defined in Eq. 15
t^* = time
t = dimensionless time = v t^*/L
T = period
T_0 = reference temperature C
v = gas flow rate
V = volume of the reactor
y = conversion = $(C_{in} - C)/C_{in}$
z^* = axial coordinate
z = dimensionless axial coordinate = z^*/L
Z_2 = cyclic group

Vector and matrix

$\boldsymbol{F}$ = vector field
$\boldsymbol{x}$ = state vector
$\boldsymbol{\lambda}$ = parameter vector

Greek letters

η = effectiveness factor
ΔH = heat of reaction
$\boldsymbol{\theta}$ = dimensionless temperature = $\gamma(T - T^0)/T^0$
ε = reactor void fraction
ε_s = catalyst porosity
ρ = density
τ = dimensionless impact time
ν = discrete variable
$\Phi_{0,\tau}$ = evolution operator of the unforced system
Π = switch map defined in Eqs. 16–17

Subscripts and superscripts

c = refers to heat exchanger
g = gas phase
h = energy balance
in = feed
m = mass
out = outlet from the system
set = set-point value
s = solid phase
w = wall

Literature Cited

1. Kolios G, Frauhammer J, Eigenberger G. Autothermal fixed-bed reactor concepts. *Chem Eng Sci*. 2000;55(24):5945.
2. Matros YuSh, Bunimovich GA. Reverse-flow operation in fixed bed catalytic reactors. *Catal Rev Sci Eng*. 1996;38:1.
3. Luss D. Temperature fronts and patterns in catalytic systems. *Ind & Eng. Chem Res*. 1997;36(8):2931.
4. Sapunzhiev C, Chaouki J, Guy C, Klvana D. Catalytic combustion of a natural-gas in a fixed bed reactor with a flow reversal. *Chem Eng Comm*. 1993;125:171.
5. Nieken U, Kolios G, Eigenberger G. Control of the ignited steady state in autothermal fixed-bed reactors for catalytic combustion. *Chem Eng Sci*. 1994;49:5507.
6. Nieken U, Kolios G, Eigenberger G. Fixed-bed reactors whit periodic-flow reversal- experimental results for catalytic combustion. *Catalysis Today*. 1994;20;335
7. Budman H, Kzyonsek M, Silveston P. Control of a nonadiabatic packed bed reactor under periodic flow reversal. *Can. J. of Chem Eng*. 1996;74(5):751.
8. Cunill F, vandeBeld L, Westerterp KR. Catalytic combustion of very lean mixtures in a reverse flow reactor using an internal electrical heater. *Ind & Eng Chem Res*. 1997;36(10):4198.
9. Dufour P, Touré Y. Multivariable model predictive control of a catalytic reverse flow reactor. *Comp Chem Eng*. 2004;28:2259.
10. Edouard D, Hammouri H, Zhou XG. Control of a reverse flow reactor for VOC combustion. *Chem Eng Sci*. 2005;60(6):1661.
11. Hevia MAG, Ordonez S, Diez FV, Fissore D, Barresi AA. Design and testing of a control system for reverse-flow catalytic afterburners. *AICHE J*. 2005:51(11);3020.
12. Barresi AA, Vanni M. Control of catalytic combustors with periodical flow reversal. *AIChE J*. 2002;48;648.
13. Schumacher H, Van der Schaft A. *Introduction to hybrid systems*. New York: Springer & Verlag: 2000.
14. Engell S, Kowalewski S, Schulz C, Sturseberg O. Continuous-discrete interactions in chemical processing plants. *Proc IEEE*. 2000; 88(7):1050.
15. Barton PI, Pantelides CC. Modelling of combined discrete-continuous process. *AIChE J*. 1994;40(6):966.
16. Bemporad A, Morari M. Control of systems integrating logic, dynamics, and constraints. *Automatica*. 1999;35(3):407.
17. Moudgalya KM, Ryali V. A class of discontinuous dynamical systems I. An ideal gas-liquid system. *Chem Eng Sci*. 2001;56:3595.
18. Moudgalya KM, Ryali V. A class of discontinuous dynamical systems II. An industrial slurry high density polyethylene reactor. *Chem Eng Sci*. 2001;56:3611.
19. El-Farra NH, Christofides PD. Coordinating feedback and switching for control of hybrid Nonlinear processes. *AIChE J*. 2003;49(8): 2079.
20. El-Farra NH, Gani A, Christofides PD. Analysis of mode transitions in biological networks. *AIChE J*. 2005;51(8):2220.
21. Khinast J, Jeong YO, Luss D. Dependence of cooled reverse-flow reactor dynamics on reactor model. *AIChE J*. 1995:45(2);299.
22. Řeháček J, Kubíček M, Marek, M. Periodic, quasi-periodic and chaotic spatio-temporal patterns in a tubular catalytic reactor with periodic flow reversal. *Comp Chem Eng*. 1998;22:283.
23. Robinson JC. *Infinite-Dimensional Dynamical Systems – An introduction to dissipative parabolic PDEs and the theory of global attractors*, Cambridge: Texts in Applied Mathematics; 2001.
24. Filippov AF. *Differential Equations with Discontinuous Righthand Sides*. Dordrecht: Kluwer Academic Publisher; 1988.
25. Lygeros J, Johansson KH, Simić NS, Zhang J, Sastry S. Dynamical properties of hybrid automata. *IEEE T Automat Contr*. 2003;48(1):2.
26. Branicky MS, Borkar VS, Mitter SK. A unified framework for hybrid control: Model and optimal control theory. *IEEE Transactions on Automatic Control*. 1998;43(1):31.
27. Johansson KH., Egerstedt M, Lygeros J, Sastry S. On the regularization of Zeno hybrid automata. *Sys & Contr Letts*. 1999;38:141.
28. Heymann M, Lin F, Meyer G, Resmerita S. Analysis of Zeno behaviours in a class of hybrid systems. *IEEE Trans on Autom Contr*. 2005;50(3):376.
29. Zhang J, Johansson KH, Lygeros J, Sastry S. Dynamical systems revisited: Hybrid systems with Zeno executions. *Lecture Notes in Comp Sci*. 2000;1790:451.
30. Zhang J, Johansson KH, Lygeros J, Sastry S. Zeno hybrid systems. *Int J Robust Nonlin*. 2001;11;435.
31. Çamlibel MK, Schmacher JM. On the Zeno behaviour of linear complementary systems. *Proc of the 40th IEEE Conference on Decision and Control*, Orlando, FL. 2001:346.
32. Golubitsky M, Stewart I. *From equilibrium to chaos in phase space and physical space*. Berlin: Birkhauser Verlag; 2000.
33. Russo L., Mancusi E, Maffettone PL, Crescitelli S. Symmetry properties and bifurcation analysis of a class of periodically forced reactors. *Chem Eng Sci*. 2002;57:5065.
34. Miller W. *Symmetry groups and their applications*. New York: Academic Press; 1972.
35. Kuznetsov, YA. *Elements of applied bifurcation theory*. 2nd ed. New York: Springer & Verlag; 1998.
36. di Bernardo M, Vasca F. On discrete time maps for the analysis of bifurcations and chaos in DC/DC converters. *IEEE Trans Circ Syst*. 2000;47:170.
37. di Bernardo M, Johansson KH, Vasca F. Self-oscillations and sliding in relay feedback systems: Symmetry and bifurcations. *Intl J of Bifurcations and Chaos*. 2001;11:1121.
38. Swift JW, Wiesenfeld K. Suppression of period doubling in symmetric systems. *Phys Rew Let*. 1984;52:705.
39. Nikolaev EV, Shnol EE. Bifurcations of cycles in systems of differential equations with a finite symmetry group - I. *J Dynam and Control Syst*. 1998;4:315.
40. Nikolaev EV, Shnol EE. Bifurcations of cycles in systems of differential equations with a finite symmetry group - II. *J Dynam and Control Syst*. 1998;4;343.
41. Villadsen J, Michelsen ML. *Solution of Differential Equation Models by Polynomial Approximation*. Prentice-Hall, Englewood Cliffs; 1978.
42. Doedel EJ, Champneys AR, Fairgrieve TF, Kuznetsov YA, Sanstede B, Wang X. AUTO97: continuation and bifurcation software for ordinary differential equations. July 1997.
43. Brown PN, Byrne GD, Hindmarsh AC. VODE: a variable coefficient ODE solver. *SIAM J Sci Stat Comput*. 1989;10:1038.

Manuscript received Nov. 17, 2006, and revision received Apr. 16, 2007.